Journal of Materials Chemistry C

Accepted Manuscript

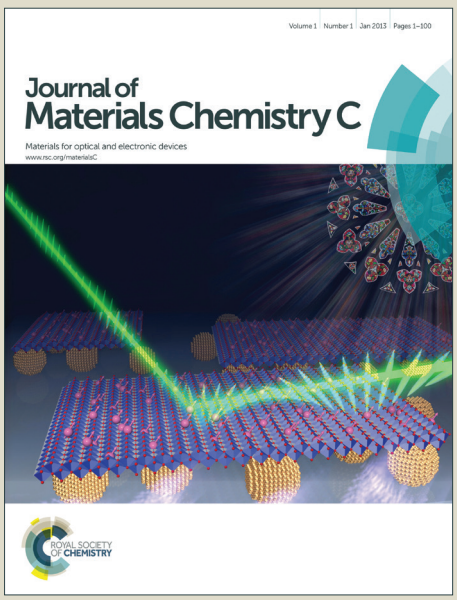

ROYAL SOCIETY OF CHEMISTRY

www.rsc.org/materialsC

Efficient 8-oxyquinolinato emitters based on 9,10-dihydro-9,10-diboraanthracene scaffold for applications in optoelectronic devices

Krzysztof Durka,[a] Ireneusz Głowacki,[b,*] Sergiusz Luliński,[a,*] Beata Łuszczyńska,[b] Jaromir Smętek,[a] Paweł Szczepanik,[a] Janusz Serwatowski,[a] Urszula E. Wawrzyniak,[c] Grzegorz Wesela-Bauman,[a,d,*] Ewelina Witkowska,[b] Gabriela Wiosna-Sałyga[b] and Krzysztof Woźniak[d]

[a]*Physical Chemistry Department, Faculty of Chemistry, Warsaw University of Technology, Noakowskiego 3, 00-664 Warszawa, Poland*
[b]*Department of Molecular Physics, Faculty of Chemistry, Lodz University of Technology, Żeromskiego 116, 90-924 Łódź, Poland*
[c]*Department of Microbioanalytics, Faculty of Chemistry, Warsaw University of Technology, Noakowskiego 3, 00-664 Warszawa, Poland*
[d]*Laboratory of Crystallochemistry, Department of Chemistry, University of Warsaw, Pasteura 1, 02-093 Warszawa, Poland.*

Corresponding authors: ireneusz.glowacki@p.lodz.pl, serek@ch.pw.edu.pl, grzegorz.wesela@chem.uw.edu.pl

Abstract

A detailed experimental characterization and theoretical evaluation of optical as well as other relevant physicochemical properties of a series of 9,10-dihydro-9,10-diboraanthracene bis(8-oxyquinolinates) and a few other related systems is reported. The obtained compounds exhibit green luminescence with quantum yields of emission up to 63% in CH_2Cl_2. Single crystal X-ray diffraction studies indicate that 9,10-dihydro-9,10-diboraanthracene complexes exist either as *bent* conformers (stabilized by a weak intramolecular CH…O interaction bringing two 8-oxyquinolinato ligands closer to each other) or *symmetrical* ones (bearing both ligands related by the centre of symmetry and separated one from the other). Theoretical calculations revealed that the LUMO levels are lower for the *bent* conformers than for the *symmetrical* ones. This suggests that the luminescent properties of the studied compounds are affected by their specific structural properties. The obtained compounds were used as emitters for the construction of organic light emitting diodes (OLEDs). The highest luminance of *ca.* 2,000 $cd \cdot m^{-2}$ was recorded for the device containing only 2.0 wt% of 1,6-difluoro-9,10-dihydro-9,10-diboraanthracene core in the poly(*N*-vinylcarbazole/2-*t*-butylphenyl-5-biphenyl-1,3,4-oxadiazole (PVK:PBD) matrix. The fabricated OLEDs exhibit current efficiency in the range from 0.5 to 1.1 $cd \cdot A^{-1}$.

Keywords: 9,10-diboranthracenes, borinic acids, 8-oxyquinolinato complexes, luminescence, optoelectronic devices

Introduction

Metal complexes with 8-oxyquinolinato ligands (Q), including boron-based systems, have been widely investigated for their potential applications in organic light emitting diodes (OLEDs).[1–11] These studies originated from a discovery of potent luminescent properties of an aluminium complex AlQ_3.[12,13] Subsequently, boron compounds turned out to be more resistant to hydrolysis[14] and more efficient emitters[15,16] than their Al counterparts. However, recent advances in the chemistry of Al derivatives showed that their stability and light-emitting properties can be greatly improved.[17–21] Various modifications of borinic systems changed their emission colour within a wide range while sustaining high quantum yields of emission (Φ).[4,6,22–26] To the best of our knowledge, the highest Φ value for a discrete borinic Q complex was 39%[22] whereas it was doubled (Φ = 80%) for one of the organoboron polymers.[1,2]

Currently, the 9,10-dihydro-9,10-diboraanthracene (DBA) derivatives have attracted significant attention due to their applications in organic synthesis and catalysis.[27–32] They were also employed in materials chemistry for the construction of n-type semiconductors[33,34] and light-emitting polymers[35–38] which exhibit photoluminescence.[34–44] Heteronuclear analogues of DBA, namely dibenzosilaborins, dibenzoazaborins, dibenzophosphaborins and dibenzochalcogenaborins (oxa, thia, selena), were also studied extensively for their applications in analytical chemistry (fluoride and cyanide ion sensors) and as strong light emitters.[45–50] In addition, Jäkle and co-workers developed synthesis and revealed crystal structure of diboradiferrocene derivatives.[51]

As a part of our interest in organoboron luminescent materials,[4,52–54] we present in this contribution UV-Vis, structural, physicochemical and theoretical studies of selected halogenated DBA derivatives with 8-oxyquinolinato ligands, **1-7**, and a few related systems **8-10** (**Scheme 1**). Based on the structure-properties relationships, we discuss the impact of the molecular conformation on the luminescence properties of the studied compounds. Finally, the selected DBA derivatives were investigated for their applications in organic light emitting diodes (OLEDs). They were used as light-emitting guest molecules in a polymeric composite host material poly(*N*-vinylcarbazole)/2-*t*-butylphenyl-5-biphenyl-1,3,4-oxadiazole (PVK:PBD).

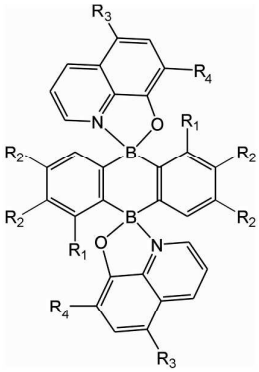

	R_1	R_2	R_3	R_4
1	H	H	H	H
2	F	H	H	H
3	Cl	H	H	H
4	Br	H	H	H
5	H	F	H	H
6	F	H	Cl	H
7	F	H	Cl	Cl

1-7

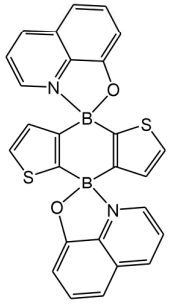

8

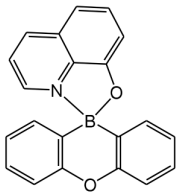

9

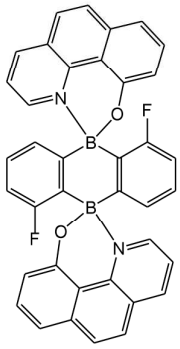

10

Scheme 1. Structures of the studied boron complexes.

Results and Discussion

Synthesis

The synthesis of complexes **1-4** was reported in our recent paper.[55] The synthesis of novel DBA derivatives **5-7** followed the same protocol. Compounds **8** and **9** were obtained by complexation of their respective precursors whose syntheses were reported previously.[56,57] In the case of **10**, benzo[h]quinolin-10-ol was used as a complexing agent instead of 8-hydroxyquinolines. In addition, we have demonstrated that the synthesis of **2** can also be accomplished using a solvent-free mechanochemical approach[58,59] by simply grinding the DBA precursor and HQ with mortar and pestle. This was evidenced by the comparison of IR spectra of samples obtained using either the mechanochemical or the standard "wet" method (**Figure S1** in the Supporting Information). All studied complexes melt at high temperatures (340−460 °C) which makes them suitable for preparation of thin layers by thermal evaporation techniques.

Crystal structure analysis

The X-ray crystal structures were determined for **1**, **2** (two crystallographic forms – **2a**, **2b**), **3**, **5** and **8**. Details for all studied compounds including molecular graphs (**Figure S6**)

and packing diagrams (**Figure S7**) are provided in the Supporting Information. The analyses of complexes bearing two Q ligands revealed that molecules can adopt either *symmetrical* or *bent* conformation. In the *symmetrical* conformation, the DBA core is essentially planar (structures **2b** and **8**), whereas this is not the case for the *bent* one where an intramolecular C−H…O interaction ($d_{C...O}$ = 3.052(2)÷3.357(2) Å, $d_{H...O}$ = 2.180÷2.515 Å) between two Q moieties occurs (**1**, **2a**, **3** and **5**). This is especially noticeable for compound **2**, where fast crystallization (*ca.* 5 hours) from $CHCl_3$ solution leads to the formation of *symmetrical* conformer **2b**, whereas the slow evaporation of acetone solution (*ca.* 1 week) results in the *bent* form **2a** (**Figure 1**). In addition, the Q ligand, which plays a donor role in the C−H…O interaction, is significantly shifted toward the second Q moiety. It is also worth noting that the crystals **2b** built up by *symmetrical* conformers incorporate solvent molecules during crystallization, whereas the molecules of *bent* conformer **2a** form a more compact, solvent-free structure. We have also noticed that the crystals of **2b** gradually lose their crystallinity, which may be attributed to solvent evaporation and plausible rearrangement to **2a**.

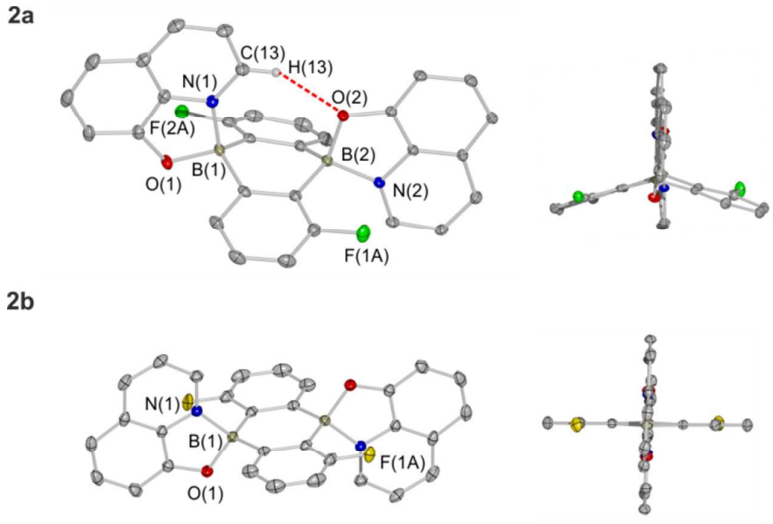

Figure 1. Labelling of atoms (only symmetrically non-equivalent heteroatoms) and estimation of atomic thermal motion as ADPs (50% probability level) together with views along two boron atoms showing two conformers of **2**. The intramolecular C−H…O contact in **2b** is shown as dashed red line. Solvent molecules (**2b**) and hydrogen atoms (except H(13) in **2b**) are omitted for clarity.

In order to establish the relative stabilities of molecular conformers of **1**, **2** and **4**, we have performed quantum-chemical computations at the RB3LYP/6-31+g(d,p) level of theory. The starting geometries were taken directly from crystal structures (after normalizing the C−H

bond distances to standard neutron values). We have traced how the energy of the molecule changes with the conformation going from *symmetrical* to *bent* by performing a constrained optimisation energy scan along the CH…O bond. This was complemented by analysis of the molecular charge density distributions within Bader's QTAIM theory[60] with the *AIMall*[61] suite of programs (all data are provided in the Supporting Information). According to the calculations, the *bent* conformer is slightly more stable (up to 5 kJ·mol^{-1} for **1**) than the *symmetrical* one (**Figure S8**). This can be rationalized by the formation of an intramolecular CH…O hydrogen bond. However, based on the Espinosa-Lecomte approximation[62–64] the stabilization provided by this interaction (*ca*. 27–37 kJ·mol^{-1}, **Table S10-S11**) should be higher. Apparently, it is compensated by other energetically unfavourable conformational effects whose nature is not clear yet. Moreover, there is essentially no barrier for the interconversion between two forms. Obviously, an important question is whether the structural flexibility of DBA Q derivatives may be reflected in their optical properties.

Electrochemical properties

The HOMO and LUMO energy values for **1-6**, and **8** were determined based on corresponding peak potentials (oxidation – E_{ox} and reduction – E_{red}) obtained using cyclic voltammetry (CV) measurements and reported with respect to the $FeCp_2/FeCp_2^+$ redox couple (**Table 3**). All compounds showed Q-ligand-centered oxidation at high positive potentials and reduction at low potentials (selected CV curves are shown in **Figure 2**, whereas data for all compounds are depicted in **Figure S2**). The electrochemical band gaps ΔE are not strongly influenced by substitution of DBA core (3.12−3.33 eV). A slightly smaller ΔE was found for **8**, whereas a wider band gap was determined for **6** bearing a 5-Cl-Q ligand. Lack of a cathodic peak corresponding to oxidation peaks at positive potentials, and lack of an anodic peak corresponding to reduction at negative potentials (especially for **1**, **2**, **4**, **6** and **8**) suggest that the studied redox processes are probably followed by chemical reactions. The use of faster scan rates did not improve their reversibility. The chemical reactions affect the shift of oxidation peaks towards less positive values, and the reduction peak towards less negative potentials. Therefore, the approximate potentials (not real formal potentials) were used to calculate the HOMO-LUMO energy levels.

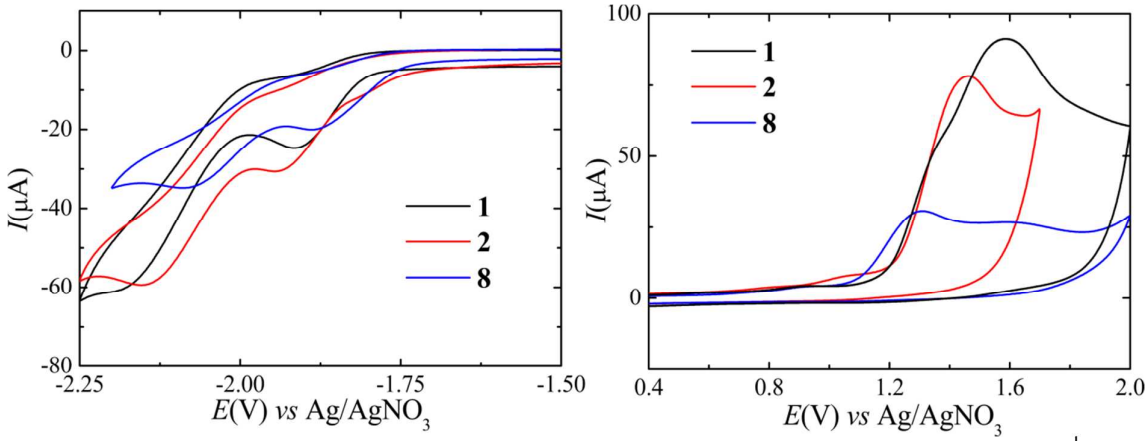

Figure 2. Cyclic voltammograms of **1**, **2** and **8** (1 mM) in Bu_4NPF_6/CH_2Cl_2, v = 0.1 V·s^{-1}.

Table 3. Energies of HOMO and LUMO levels (eV) for **1-6** and **8** based on CV measurements.

	E_{HOMO}	E_{LUMO}	ΔE
1	−6.03	−2.70	3.33
2	−5.91	−2.79	3.12
3	−5.93	−2.69	3.24
4	−5.90	−2.68	3.22
5	−5.96	−2.71	3.25
6	−6.32	−2.87	3.45
8	−5.75	−2.76	2.99

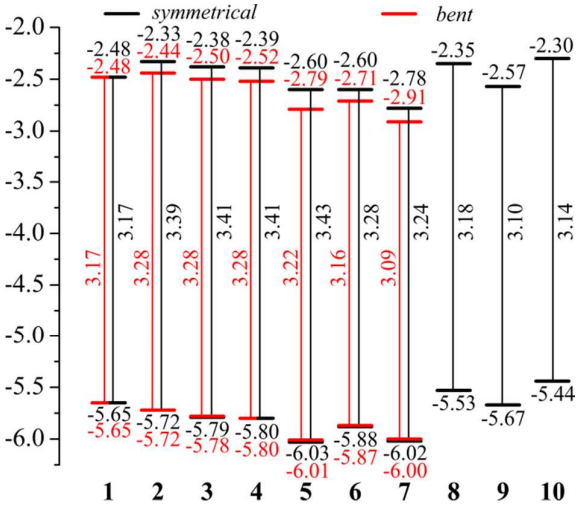

Figure 3. Energies of frontier orbitals (eV) for **1-10** calculated at the TD-RB3LYP/6-31+g(d,p) level of theory.

Optical properties and computational studies

The optical properties of compounds **1-10** were investigated by UV-Vis absorption and photoluminescence spectroscopy in CH_2Cl_2 solution at ambient conditions and the data

are provided in **Table 4**. A plot of the recorded spectra is depicted in **Figures 4a** and **4b**. Experimental results were supported by computational TD-DFT studies. Experimental and theoretical details of electron excitations and relaxations are summarized in the Supporting Information (**Table S3-S4**).

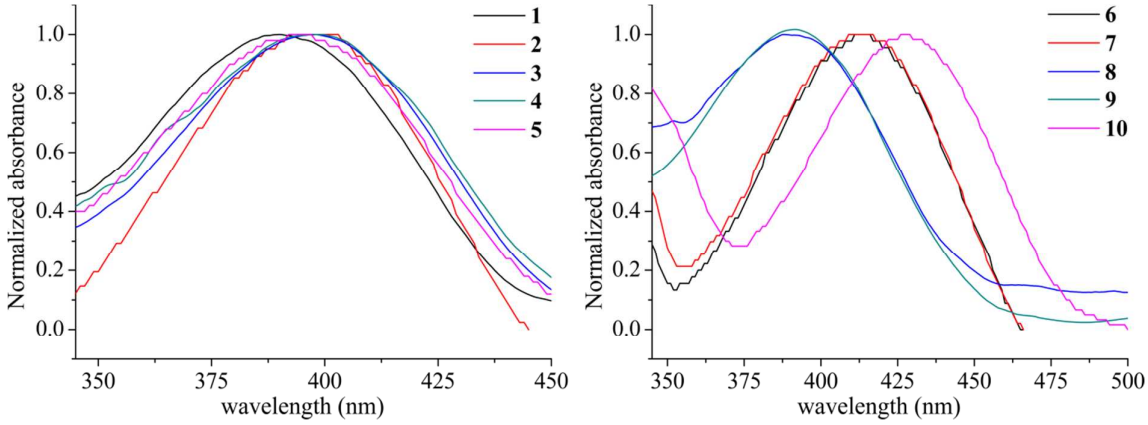

Figure 4a. Normalized absorption of **1-10** recorded in CH_2Cl_2.

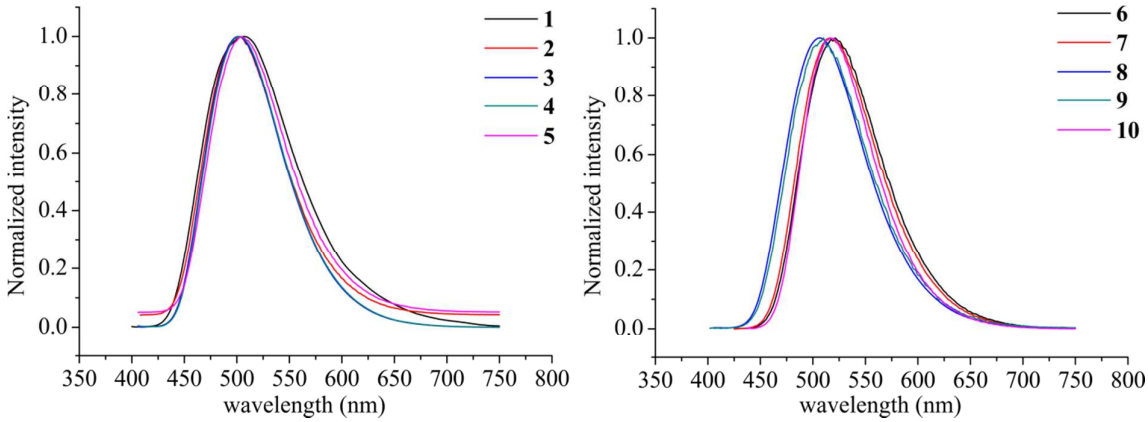

Figure 4b. Normalized emission of **1-10** recorded in CH_2Cl_2.

The studied complexes have long-wave absorption and emission bands in the range of 390-427 nm and 494-522 nm, respectively. Similar spectral features were reported for the reference compound **Ph_2BQ** (λ_{max}= 396 nm, λ_{em}= 504 nm).[6] Specifically, DBA derivatives were found to be very good emitters with quantum yield of 63% for **5**, which significantly exceeds the values reported for **Ph_2BQ**. These Φ values are, to the best of our knowledge, the highest figures obtained for non-polymeric borinic 8-oxyquinolinates. We were interested to check how the optical properties are influenced by replacement of the DBA core and Q with related moieties. The use of 5-Cl-Q or BQ ligands instead of Q (**2** *vs* **6** or **10**) resulted in lowering of Φ values in accordance with previous reports.[4,5,22] The relative decrease of fluorescence for emitters **6–7** could be attributed to increased contributions of n–π* transitions

arising from the presence of chlorine atoms (**Table S5-S6**). The moderate emission of thiophene- (**8**) and oxaborin-based (**9**) systems can be rationalized in terms of a similar quenching mechanism invoked for **6-7**. It is also plausible that the lower Φ value for **9** is due to its single-chromophore structure.

Table 4. Experimental and calculated photophysical properties of **1-10**. Calculations were done at the TD-RB3LYP/6-31+g(d,p) level of theory.

	Experimental data					TD-DFT calculations	
Compound	λ_{max} [nm]	ε [M^{-1} cm^{-1}]	λ_{em} [nm]	Δ [nm]	Φ [a] [%]	$\lambda_{max}(f)$ [b] [nm]	$\lambda_{em}(f)$ [b] [nm]
Ph_2BQ[6,26,65]	396	-	504	108	30	416(--)	516(--)
1	390	4600	494	104	48	427(0.050) / --	486(0.045) /--
2	397	8200	503	106	52	442(0.085) / 440(0.123)	-- / 567(0.046)
3	396	7100	502	106	53	442(0.075) / 439(0.116)	564(0.048) /--
4	396	3800	502	106	41	442(0.070) / 440(0.115)	564(0.046) / 574(0.042)
5	396	10000	504	108	63	421(0.042) /--	-- / --
6	414	9000	522	108	13	460(0.106) / 459(0.149)	604(0.053) / --
7	414	9400	516	102	26	467(0.089) / 464(0.141)	528(0.047) / --
8	392	4800	506	114	22	-- / 426(0.13)	482(0.078) / --
9	390	4200	510	120	19	430(0.055)	--
10	427	12000	520	93	19	-- / 473(0.081)	-- / --

[a] Excited at the absorption maximum at the longest wavelength (solvent CH_2Cl_2, $c = 5 \times 10^{-5}$ M; standard: Coumarine 153 in EtOH, $c = 5 \times 10^{-6}$ M, rt). [b] data obtained for *bent* /*symmetrical* conformation. Δ denotes the Stokes shift.

In the next step, the spectroscopic measurements for layers of the PVK:PBD blends doped with the complexes **1** and **2** were carried out. The emission maxima for these materials are similar to the ones observed for solutions **1** and **2**. Upon excitation with light of 340 nm, corresponding to the lowest energy absorption band of PVK:PBD matrix, the Φ values for layers doped with **1** and **2** were equal to 43% and 41%, respectively (**Figure 4c**).

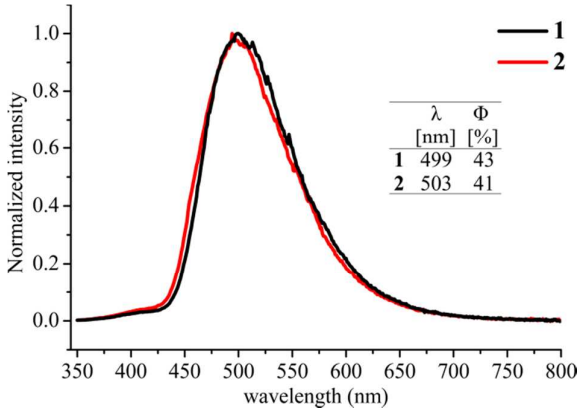

Figure 4c. Normalized emission of **1** and **2** recorded in PVK:PBD matrix (excitation with light of 340 nm).

Thin layer Φ values were similar to the ones observed for the respective solutions. Such high values of Φ for the thin films indicate an effective process of excitation energy transfer from the matrix to dopant molecules which can be rationalized by a good spectral overlap of the emission band of PVK:PBD and the absorption band of the dopants. The values of spectral overlap integral (*J*, calculated according to published procedure[66]) between host and guest were determined as 4.82 and $7.61 \cdot 10^{13}$ nm^4 $M^{-1}cm^{-1}$; consequently, the Förster radii (R_0) were 1.8 and 1.9 nm for **1** and **2**, respectively. Thus, one can assume a Förster mechanism of energy transfer.

Theoretical spectra simulated with the TD-B3LYP/6-31+g(d,p) method reproduce experimentally observed trends, although predicted values deviate from experimentally observed ones (**Table 4**). A complete set of theoretical data related to light absorption and emission is given in **Table S3-S5**. For some compounds we were not able to establish fully-optimized *bent* or *symmetrical* forms either in ground or excited states. Computations revealed that spectral bands of the *bent* and *symmetrical* conformations can differ slightly. At this point, we cannot unambiguously determine which form persists either in solution or in prepared OLED layers. However, we have observed a similar values of Stokes shifts for **1**-**7** which indicates a similar excitation pathways. It is plausible that the studied systems may undergo *bent*/*symmetrical* form transformation (*e.g.*, in solution) during the process of electron excitation/relaxation. To illustrate this phenomenon, the possible transformations along with frontier orbitals for compounds **2**, **4** and **8** are shown in **Figure 5**. For compound **2** both conformations for ground state and only *symmetrical* excited state form were established. For compound **4** both conformations for ground state and excited state were found. The theoretical ground state optimization of **8** revealed that it is a *symmetrical* conformer and the stable excited state conformation is the *bent* one which is in line with the increased Stokes shift for this system with respect to **1**-**7**. Significant changes of the geometry during light excitation/emission can be expected for **9** where we have observed the largest Stokes shift. On the other hand switching from Q to BQ (**10**) yielded in the smallest Δ value.

The distribution of frontier orbitals changes when DBA systems rearrange from *symmetrical* to *bent* forms. For the *symmetrical* form, both Q rings are equally involved in creating HOMO and LUMO orbitals. In contrast, in the *bent* form the HOMO orbital spans across the one of Q ligands (intramolecular C−H...O H-bond donor) while the LUMO orbital is spread onto the second Q ligand (H-bond acceptor). Switching to a *bent* geometry stabilizes

the LUMO orbital by *ca*. 0.1−0.2 eV and hence the HOMO-LUMO energy gap decreases, leading to red-shifted absorption bands. Halogenation of DBA cores stabilizes HOMO level due to electron withdrawal resulting in the increased HOMO-LUMO energy gap. Narrowing of the band gap was found for **8** where switching from benzene to thiophene rings increased the HOMO energy while destabilizing the LUMO level.

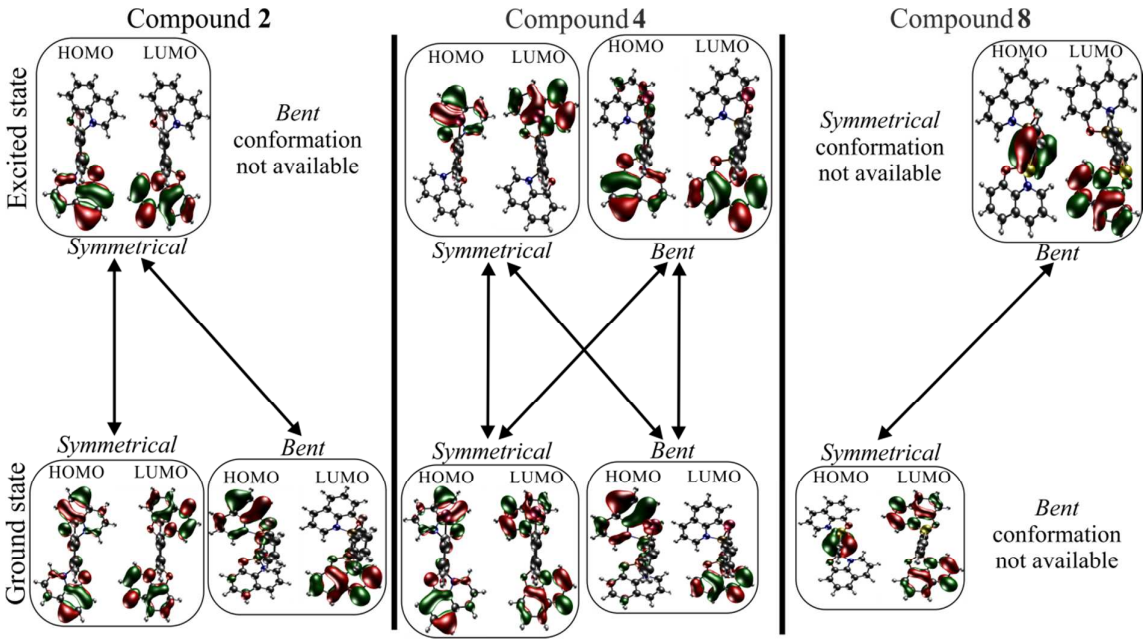

Figure 5. Plot of molecular orbitals of compounds **2**, **4** and **8**. Arrows indicates possible changes of conformation during processes of electron excitation and relaxation.

In addition, inner reorganization energies (Λ) were calculated for obtained systems (**Table S9**) and compared with the commonly used charge carrier AlQ_3.[67] The results indicate that our systems, especially in the *symmetrical* form, can be excellent materials for transporting both holes and electrons as their Λ values calculated within the framework of Marcus theory are lower than those obtained for AlQ_3.

Preparation and characterization of OLEDs

OLEDs were constructed using a combination of spin-coating and solvent evaporation techniques followed by encapsulation. Emitting compounds (**1** or **2**) were blended with a PVK:PBD matrix and put between a hole injecting layer (HIL) composed of poly(3,4-ethylenedioxythiophene):sodium poly(styrene sulfonate) mixture (PEDOT:PSS) and an electron injecting layer (EIL, Al/LiF) as shown in **Figure 6**.[68] Current-voltage (*I-V*) and luminance–voltage (*L-V*) characteristics of the fabricated devices exhibit typical OLED behaviour (see **Figure 7**).[69] The turn-on voltage in the range from 6 to 8 V was determined

based on the detected luminance value of 1 cd·m^{-2} (not visible in **Figure 7**, because of the presented luminance range). The highest luminance (*ca.* 2,000 cd·m^{-2} at 16 V) was obtained for a diode based on emitter **2**.

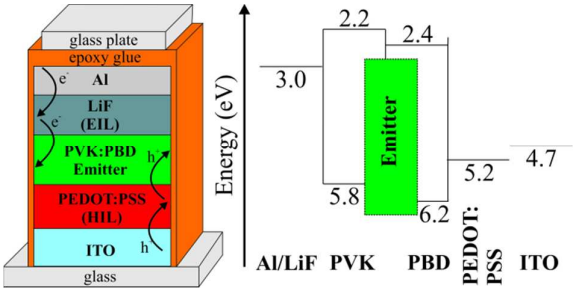

Figure 6. Scheme of layers in built diodes (left) along with energy levels of frontier orbitals of respective layers (right).

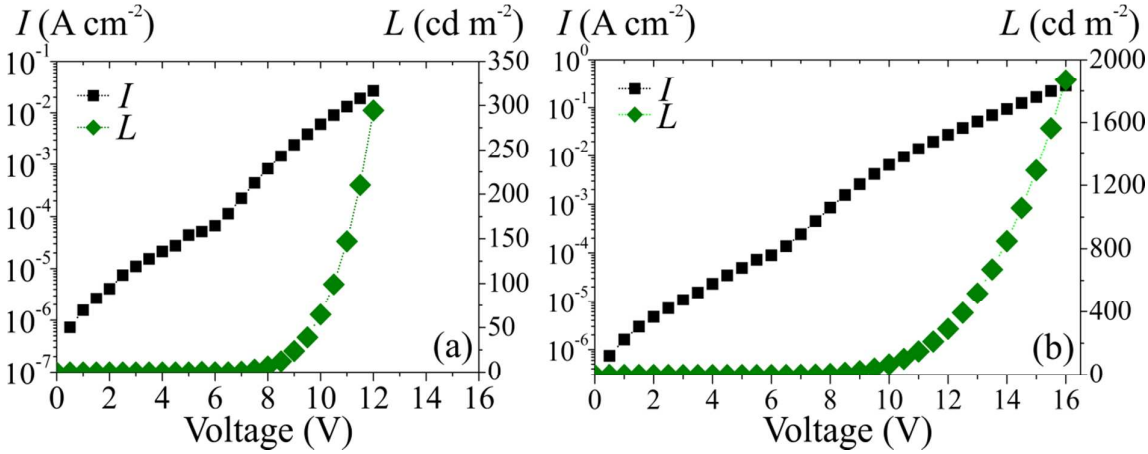

Figure 7. Current density-Voltage-Luminance (*I-V-L*) characteristics of OLED based on emitters **1** (a) and **2** (b).

The fabricated devices exhibit current efficiency in the range of 0.5–1.1 cd·A^{-1}. In **Figure 8** the current efficiencies are plotted against the current density for polymer LEDs (PLEDs) based on PVK:PBD doped with 2.0 wt% **1** or **2**. It should be emphasized that PLEDs exhibited a stable green colour of emitted light in a broad voltage range which was confirmed by control of the colour coordinates (*x*,*y*) presented in the CIE 1931 diagram (**Figure S9**). Their colour coordinates are close to those obtained for a similar diode based on the AlQ_3 emitter. Diodes built with **1** as emitter exhibited lower stability at higher voltages (above 12 V). For emitters **1** and **2**, the guest molecules constitute traps for electrons injected into the host matrix. The relative positions of the HOMO energy level of the used emitters exclude the trapping effect of the holes by the molecules of dopant. Nevertheless, the electrons trapped on the guest molecules may act as negatively charged centres which favour the transfer of holes to dopant molecules. In consequence, the charge carrier recombination takes place on the

emitter molecules which results in green emission. Moreover, the obtained EL spectra (**Figure 4c**) do not allow one to assume the creation of the most common PVK:PBD exciplexes whose presence is discussed in the literature for similar systems.[70,71] The emission of PVK-PBD exciplexes is observed at 430 nm and its presence in ternary emissive blends may indicate an incomplete transfer of the excitation energy from the matrix to the dopant. The lack of the exciplex emission in our ternary systems supports implementation of the PVK:PBD matrix.

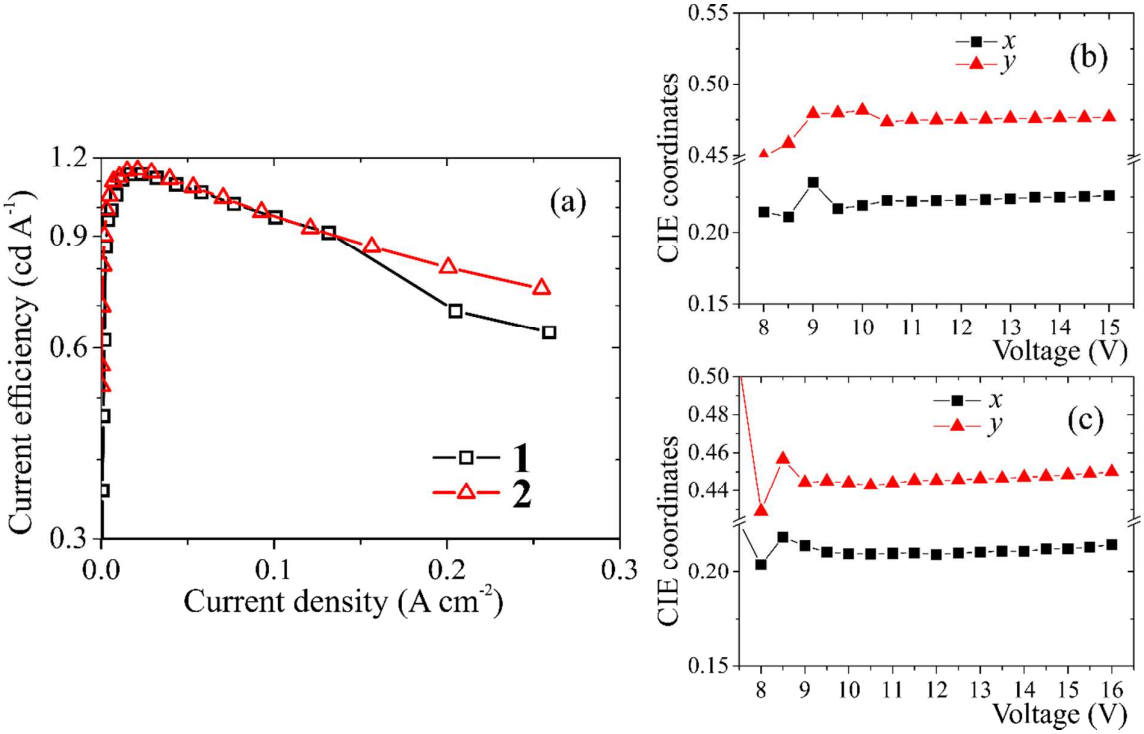

Figure 8. Current efficiency *versus* current density for **1** (black line) or **2** (red line) (a) and CIE1931(*x*,*y*) *versus* voltage for **1** (b) and **2** (c) emitters.

Conclusions

In conclusion, we have studied the luminescence properties of a series of new organoboron 8-oxyquinolinato complexes. These compounds can be obtained with good yields and exhibit relatively high melting points. Among the investigated systems, DBA Q derivatives are very efficient green emitters in solution (λ_{em}= 494−506 nm, Φ up to 63%) and in a PVK:PBD matrix (λ_{em}= 499−503 nm, Φ up to 43%). Selected complexes performed well as light emitters in OLED devices based on the PVK:PBD matrix blended with our systems. The obtained devices presented long term stability with luminances reaching *ca*. 2000 cd·m^{-2} and current efficiencies above 1 cd·A^{-1}. It should be stressed that such good parameters were achieved with diodes containing only 2 wt% of emitter in the matrix whereas in previous

reports much higher emitter contents (above 10 wt%) were used.[72] It may be the case that the promising optical properties of **1-5** are a consequence of a cooperation of two Q chromophores present in the molecular structure. The X-ray diffraction and theoretical analyses revealed that molecules of the studied complexes can adopt respective *bent* conformations (apart from the *symmetrical* ones) where one observes mutual interaction of two chromophores (Q ligands) by means of an intramolecular C–H...O hydrogen bond. Based on the results of TD-B3LYP/6-31+g(d,p) calculations, the HOMO-LUMO transition, in this case, can be reasonably interpreted as ligand-to-ligand charge transfer (LLCT). Hence, we suppose that fixing the *bent* structure (*e.g.*, by creating a covalent linker between Q rings) could result in the formation of a system featuring more strongly interacting Q chromophores and thus show optical properties even better than those reported here. Further studies on applications of DBA Q derivatives in optoelectronics are currently in progress.

Experimental Section

Synthesis and characterization of compounds 1-10. Syntheses of **1-4** were reported recently.[55,73] Complexes **5-10** were prepared on a 10 mmol scale in a simple manner by complexation of respective organoboron precursors with stoichiometric amounts of appropriate ligands in Et_2O. They were characterized by ^{1}H, ^{13}C, ^{11}B and ^{19}F NMR, elemental analyses and HRMS (ESI).

X-ray diffraction studies. The single crystals of **1**, **2a**, **2b**, **3**, **5**, **8** and **9** were obtained by slow evaporation of corresponding acetone (**1**, **2a**, **3** and **8**) or chloroform (**2b**, **5** and **9**) solutions. X-ray diffraction data sets for single crystals of **1**, **2a** and **8** were collected at 100 K on a Bruker AXS Kappa APEX II Ultra diffractometer with a TXS rotating anode (Mo-Kα radiation, λ = 0.71073 Å), multi-layer optics and equipped with an Oxford Cryosystems nitrogen gas-flow attachment. The data collection strategy was optimized and monitored using the appropriate algorithms applied in the *APEX2* program package.[74] Data reduction and analysis were carried out with the *APEX2* suit of programs (integration was done with *SAINT*).[75] The multi-scan absorption correction, scaling and merging of reflection data were done with *SORTAV*.[76,77] Single crystals of **2b**, **3**, **5** and **9** were measured on a Kuma KM4CCD κ-axis diffractometer with graphite-monochromated Mo-Kα radiation and equipped with an Oxford Cryosystems nitrogen gas-flow apparatus. Data reduction and analysis were carried out with the *CrysAlisPro* suite of programs.[78]All structures were solved by direct methods using *SHELXS-2013* and refined using *SHELXL-2013*.[79] Selected crystal

data for all crystals are summarized in **Table S2**. Crystallographic data have been deposited at CSD and the particular structures carry the following identification codes: 1023719 (**1**), 1023720 (**2a**), 1023721 (**2b**), 1023722 (**3**), 1023723 (**5**), 1023724 (**8**), 1023725 (**9**).

Optical properties. UV-Vis emission spectra were recorded using a Fluorolog 3-2-IHR320-TCSPC (from Jobin Yvon) spectrometer equipped with a photocounter and CCD detector. Detector calibration has been conducted with *Spectral Fluorescence Standard Kit*[80] certified by BAM. All emission data were collected twice with 0.5 s of integration. Emission spectra were obtained after excitation at the longest wavelength of the absorption peaks. The absorption spectra were recorded using Hitachi UV-2300 II spectrometer. Quantum yields of emission were determined using known procedures[81] based on the formula:

$$\phi = \phi_w \frac{\int I(\tilde{\nu})d\tilde{\nu}}{\int I_w(\tilde{\nu})d\tilde{\nu}} \frac{1-\mathrm{e}^{-\mathrm{A_w}}}{1-\mathrm{e}^{-\mathrm{A}}} \frac{n^2}{n_w^2}$$

where $I(\tilde{\nu})$ and $I_w(\tilde{\nu})$ are intensities of the sample and standard, respectively; A and A_w are absorbances of the sample and standard, respectively, at the wavelength at which excitation of the compound has occurred; n is the refractive index. All measurements were carried out at room temperature. The quantum yield of the reference standard Coumarine 153 was adopted from an IUPAC report ($\phi_w = 0.38$)[81] and its concentration was kept at $5 \cdot 10^{-6}$ M. Concentrations of samples of analysed compounds were kept at $1 \cdot 10^{-6}$ M.

DSC analysis. DSC measurements were performed on a DSC Q200 calorimeter from TA Instruments. Melting points (T_m), glass transition temperatures (T_g), and crystallization temperatures (T_c) were established. DSC curves are provided in the Supporting Information.

Electrochemical measurements. Cyclic voltammetry measurements were carried out using a CHI 1040 potentiostat (CH Instrument, Austin, USA) in the three electrode arrangement, with $Ag/AgNO_3$ (0.01 M) in CH_3CN as the reference, platinum rod as the counter electrode and the glassy carbon disk electrode (GCE from BASi, USA, A = 0.0706 cm^2) as the working electrode. The reference electrode was separated from the working solution by an electrolytic bridge filled with the 0.1 M Bu_4NPF_6 in CH_2Cl_2. The reference electrode potential was calibrated using a ferrocene electrode process in the same Bu_4NPF_6/CH_2Cl_2 solution with $E°(FeCp_2/FeCp_2^+)$ = 0.272 V. Potentials of all studied compounds were assigned versus the $FeCp_2/FeCp_2^+$ redox pair. Argon was used to deaerate all the studied solutions and an argon blanket was maintained over the solution during the experiments. All electrochemical experiments were carried out at 25 °C. The working electrode was sequentially mechanically polished with 1.0, 0.3 and 0.05 mm alumina powder (Buehler, Lake Bluff, IL), on a polishing cloth to a mirror-like surface. Finally, it was rinsed

thoroughly with CH_2Cl_2 and sonicated for 5 min in pure CH_2Cl_2, in order to remove remaining powder.

OLEDs fabrication and characterization processes. OLEDs were fabricated on indium tin oxide (ITO) coated glass substrates (Ossila). First, a *ca.* 30 nm thick layer of PEDOT:PSS mixture was spin-coated on top of oxygen plasma treated ITO. This substrate was annealed at 200 °C for 10 min. Then, a light-emitting layer (*ca*. 70 nm), containing PVK with 40 wt% PBD and 2.0 wt% emitter molecules was spin-coated from a chlorobenzene solution onto the baked PEDOT:PSS layer (from H. C. Starck company). PBD was used in order to improve poor electron-transporting properties of a matrix based on PVK. Previous reports show that the PVK:PBD weight ratio of 70:30 is the most optimal weight ratio of these materials taking into account the quality of thin layers and device performance.[82,83] To remove the residual amounts of the solvent, the subsequent deposited active layers were annealed at 90 °C for 30 min in a nitrogen atmosphere. After that a LiF interfacial layer (thickness of *ca*. 1 nm) was placed between the active layer and the Al electrode in order to improve electron injection from the Al cathode to the active layer. Both LiF and Al layers were deposited by a vacuum evaporation technique. The thickness of the deposited Al cathode was 100 nm. The devices had an active area of 4.5 mm^2 (3.0 mm × 1.5 mm). Finally, the devices were encapsulated with epoxy resin and glass, inside a glove box. The encapsulated OLEDs could be characterized and tested under ambient conditions. The thickness of the spin-coated layer was controlled using a Dektak XT profilometer (Bruker). The electroluminescence spectra were recorded using a MicroHR spectrometer and a CCD camera 3500 (Horiba Jobin Yvon). Current-voltage-luminance characteristics were determined by using the Keithley 2400 source measurement unit and the Minolta CS-200 camera. The use of Minolta CS-200 has also allowed control of the colour stability.

Spectroscopic experiments. From the same solutions used for fabrication of emissive layers in OLEDs, thin layers on quartz substrates were deposited with a spin speed of 2000 rpm for spectroscopic experiments. Photoluminescence (PL) spectra were recorded on Edinburgh Instruments FLS980 spectrofluorimeter. The photoluminescence quantum yield measurements of the emissive layers were done using an integrating sphere provided by Edinburgh Instruments. All films were excited at absorption maximum (340 nm) of PVK:PBD matrix. UV-Vis absorption spectra were recorded using a Varian Cary 5000 spectrophotometer.

Theoretical calculations. Optimizations of molecular geometries were conducted using experimental X-ray geometries as starting points at RB3LYP/6-31+g(d,p) and

UB3LYP/6-31+g(d,p) levels of theory for all compounds. For compounds for which X-ray geometries had not been determined, full optimizations were conducted at the same level. In all cases C–H bond lengths were fixed to standard neutron distances (1.083 Å)[84] prior to optimization. Unrestricted DFT calculations were checked against spin contamination. Excited state geometries, along with absorption and emission spectra, were obtained using TD-DFT methods with the same basis set, using geometries obtained from ground state optimizations. After geometry optimization, the vibrational frequencies were calculated and the results showed that optimized structures are stable geometric structures. Tight convergence criteria were used along with high precision integrals (*int=UltraFine*) to obtain good quality wave functions. Default criteria were used for the constrained optimisation scans. In all cases wave functions were calculated without the use of symmetry constraints. All calculations were performed using the *Gaussian09*[85] suits of programs. The *VMD* program was used for visualization of molecular orbitals[86]. Evaluation of the charge transport properties was done with Marcus theory.[87,88] Cartesian coordinates of molecules in ground states (calculated with restricted and unrestricted level of theory), molecules in the first excited states, geometries of charged molecules (both as cationic and anionic species) and geometries taken from constrained optimization scans are in the Supporting Information.

Electronic supplementary information (ESI) available: Experimental procedures and characterization for all new compounds, X-ray structural, electrochemical and spectral data, and details of quantum-chemical calculations are provided (132 pages) (PDF).

Acknowledgements

This work was supported by the National Science Centre (Narodowe Centrum Nauki, Grant No. DEC-2011/03/B/ST5/02755). The support by Aldrich Chemical Co., Milwaukee, WI, U.S.A., through continuous donation of chemicals and equipment is gratefully acknowledged. Authors thank The Interdisciplinary Centre of Mathematical and Computational Modelling in Warsaw (grant no. G33-14) for providing computer facilities on which most of the calculations were done. G. Wesela-Bauman thanks the Foundation for Polish Science for financial support within the International PhD Program. The MPD/2010/4 project is realized within the MPD programme of Foundation for Polish Science, cofinanced by the European Union, Regional Development Fund. G. Wiosna-Sałyga acknowledges the financial support of the National Science Centre (Poland) through the Grant No. 2012/04/S/ST4/00128. Authors are grateful to Dr. Siân T. Howard for reading and correcting the manuscript.

References

1. K. Tanaka and Y. Chujo, *Macromol. Rapid Commun.*, 2012, **33**, 1235–1255.
2. Y.-L. Rao and S. Wang, *Inorg. Chem.*, 2011, **50**, 12263–12274.
3. F. Jäkle, *Chem. Rev.*, 2010, **110**, 3985–4022.
4. G. Wesela-Bauman, P. Ciećwierz, K. Durka, S. Luliński, J. Serwatowski and K. Woźniak, *Inorg. Chem.*, 2013, **52**, 10846–10859.
5. Y. Tokoro, A. Nagai, K. Kokado and Y. Chujo, *Macromolecules*, 2009, **42**, 2988–2993.
6. Y. Cui, Q.-D. Liu, D.-R. Bai, W.-L. Jia, Y. Tao and S. Wang, *Inorg. Chem.*, 2005, **44**, 601–609.
7. Y. Tokoro, A. Nagai and Y. Chujo, *Appl. Organomet. Chem.*, 2010, **24**, 563–568.
8. F. Jäkle, *Coord. Chem. Rev.*, 2006, **250**, 1107–1121.
9. A. Nagai and Y. Chujo, *Chem. Lett.*, 2010, **39**, 430–435.
10. H. Li and F. Jäkle, *Angew. Chem. Int. Ed.*, 2009, **48**, 2313–2316.
11. D. Frath, J. Massue, G. Ulrich and R. Ziessel, *Angew. Chem. Int. Ed.*, 2014, **53**, 2290–2310.
12. C. W. Tang, S. A. VanSlyke and C. H. Chen, *J. Appl. Phys.*, 1989, **65**, 3610–3616.
13. C. W. Tang and S. A. VanSlyke, *Appl. Phys. Lett.*, 1987, **51**, 913–915.
14. J. E. Knox, M. D. Halls, H. P. Hratchian and H. B. Schlegel, *Phys. Chem. Chem. Phys.*, 2006, **8**, 1371–1377.
15. S. Anderson, M. S. Weaver and A. J. Hudson, *Synth. Met.*, 2000, **111–112**, 459–463.
16. X.-Y. Wang and M. Weck, *Macromolecules*, 2005, **38**, 7219–7224.
17. J. P. Heiskanen, A. E. Tolkki, H. J. Lemmetyinen and O. E. O. Hormi, *J. Mater. Chem.*, 2011, **21**, 14766–14775.
18. V. Zlojutro, Y. Sun, Z. M. Hudson and S. Wang, *Chem Commun*, 2011, **47**, 3837–3839.
19. V. M. Manninen, W. A. E. Omar, J. P. Heiskanen, H. J. Lemmetyinen and O. E. O. Hormi, *J. Mater. Chem.*, 2012, **22**, 22971–22982.
20. W. A. E. Omar, *J. Adv. Res.*, 2013, **4**, 525–529.
21. N. Lin, J. Qiao, L. Duan, J. Xue and L. Wang, *Chem. Mater.*, 2014, **26**, 3693–3700.
22. Y. Qin, I. Kiburu, S. Shah and F. Jäkle, *Org. Lett.*, 2006, **8**, 5227–5230.
23. Y. Nagata and Y. Chujo, *Macromolecules*, 2008, **41**, 2809–2813.
24. Y. Cui and S. Wang, *J. Org. Chem.*, 2006, **71**, 6485–6496.
25. H. Li and F. Jäkle, *Macromolecules*, 2009, **42**, 3448–3453.
26. S. Kappaun, S. Rentenberger, A. Pogantsch, E. Zojer, K. Mereiter, G. Trimmel, R. Saf, K. C. Möller, F. Stelzer and C. Slugovc, *Chem. Mater.*, 2006, **18**, 3539–3547.
27. V. C. Williams, C. Dai, Z. Li, S. Collins, W. E. Piers, W. Clegg, M. R. J. Elsegood and T. B. Marder, *Angew. Chem. Int. Ed.*, 1999, **38**, 3695–3698.
28. M. V. Metz, D. J. Schwartz, C. L. Stern, T. J. Marks and P. N. Nickias, *Organometallics*, 2002, **21**, 4159–4168.
29. M. V. Metz, D. J. Schwartz, C. L. Stern, P. N. Nickias and T. J. Marks, *Angew. Chem. Int. Ed.*, 2000, **39**, 1312–1316.
30. S. N. Kessler, M. Neuburger and H. A. Wegner, *Eur. J. Org. Chem.*, 2011, **2011**, 3238–3245.
31. S. N. Kessler and H. A. Wegner, *Org. Lett.*, 2010, **12**, 4062–4065.
32. T. Agou, M. Sekine and T. Kawashima, *Tetrahedron Lett.*, 2010, **51**, 5013–5015.
33. J. Chai, C. Wang, L. Jia, Y. Pang, M. Graham and S. Z. D. Cheng, *Synth. Met.*, 2009, **159**, 1443–1449.

34. E. Januszewski, A. Lorbach, R. Grewal, M. Bolte, J. W. Bats, H.-W. Lerner and M. Wagner, *Chem. Eur. J.*, 2011, **17**, 12696–12705.
35. A. Lorbach, M. Bolte, H. Li, H.-W. Lerner, M. C. Holthausen, F. Jäkle and M. Wagner, *Angew. Chem. Int. Ed.*, 2009, **48**, 4584–4588.
36. F. Jäkle, *Chem. Rev.*, 2010, **110**, 3985–4022.
37. A. Lorbach, M. Bolte, H.-W. Lerner and M. Wagner, *Chem, Commun,*, 2010, **46**, 3592–3594.
38. J. Chen, J. W. Kampf and A. J. Ashe III, *Organometallics*, 2008, **27**, 3639–3641.
39. C. Hoffend, F. Schödel, M. Bolte, H.-W. Lerner and M. Wagner, *Chem. Eur. J.*, 2012, **18**, 15394–15405.
40. C. Reus, S. Weidlich, M. Bolte, H.-W. Lerner and M. Wagner, *J. Am. Chem. Soc.*, 2013, **135**, 12892–12907.
41. C. Reus, F. Guo, A. John, M. Winhold, H.-W. Lerner, F. Jäkle and M. Wagner, *Macromolecules*, 2014, **47**, 3727–3735.
42. C. Hoffend, K. Schickedanz, M. Bolte, H.-W. Lerner and M. Wagner, *Tetrahedron*, 2013, **69**, 7073–7081.
43. C. Hoffend, M. Diefenbach, E. Januszewski, M. Bolte, H.-W. Lerner, M. C. Holthausen and M. Wagner, *Dalton Trans.*, 2013, **42**, 13826–13837.
44. C. Dou, S. Saito and S. Yamaguchi, *J. Am. Chem. Soc.*, 2013, **135**, 9346–9349.
45. A. Lorbach, A. Hubner and M. Wagner, *Dalton Trans.*, 2012, **41**, 6048–6063.
46. A. Kawachi, H. Morisaki, T. Hirofuji and Y. Yamamoto, *Chem. Eur. J.*, 2013, **19**, 13294–13298.
47. T. Agou, M. Sekine, J. Kobayashi and T. Kawashima, *Chem. Eur. J.*, 2009, **15**, 5056–5062.
48. T. Agou, J. Kobayashi and T. Kawashima, *Org. Lett.*, 2005, **7**, 4373–4376.
49. T. Matsumoto, C. R. Wade and F. P. Gabbaï, *Organometallics*, 2010, **29**, 5490–5495.
50. J. Kobayashi, K. Kato, T. Agou and T. Kawashima, *Chem. Asian J.*, 2009, **4**, 42–49.
51. P. Thilagar, D. Murillo, J. Chen and F. Jakle, *Dalton Trans*, 2013, **42**, 665–670.
52. G. Wesela-Bauman, S. Luliński, J. Serwatowski and K. Woźniak, *Phys. Chem. Chem. Phys.*, 2014, **16**, 22762–22774.
53. G. J. Wesela-Bauman, S. Parsons, J. Serwatowski and K. Woźniak, *CrystEngComm*, 2014, **16**, 10780–10790.
54. G. Wesela-Bauman, L. Jastrzębski, P. Kurach, S. Luliński, J. Serwatowski and K. Woźniak, *J. Organomet. Chem.*, 2012, **711**, 1–9.
55. S. Luliński, J. Smętek, K. Durka and J. Serwatowski, *Eur. J. Org. Chem.*, 2013, **2013**, 8315–8322.
56. E. Borowska, K. Durka, S. Luliński, J. Serwatowski and K. Woźniak, *Eur. J. Org. Chem.*, 2012, 2208–2218.
57. N. L. Kostenko, S. V. Nesterova, S. V. Toldov, N. K. Skvortsov and V. O. Reikhsfel'd, *Zh. Obshch. Khim.*, 1987, **57**, 716–717.
58. S. L. James, C. J. Adams, C. Bolm, D. Braga, P. Collier, T. Friiščić, F. Grepioni, K. D. M. Harris, G. Hyett, W. Jones, A. Krebs, J. Mack, L. Maini, A. G. Orpen, I. P. Parkin, W. C. Shearouse, J. W. Steed and D. C. Waddell, *Chem. Soc. Rev.*, 2012, **41**, 413–447.
59. T. Friščić, *Chem. Soc. Rev.*, 2012, **41**, 3493–3510.
60. R. F. W. Bader, *Atoms in Molecules: A Quantum Theory*, Oxford University Press, Oxford, 1990.
61. T. A. Keith, *AIMAll*, TK Gristmill Software, Overland Park KS, USA, 2012.
62. Y. A. Abramov, *Acta Crystallogr. Sect. A*, 1997, **53**, 264–272.
63. E. Espinosa, E. Molins and C. Lecomte, *Chem. Phys. Lett.*, 1998, **285**, 170–173.
64. E. Espinosa, C. Lecomte and E. Molins, *Chem. Phys. Lett.*, 1999, **300**, 745–748.
65. Y. L. Teng, Y. H. Kan, Z. M. Su, Y. Liao, S. Y. Yang and R. S. Wang, *Theor. Chem. Acc.*, 2007, **117**, 1–5.

66. A. Visser, E. Vysotski and J. Lee, *Crit. Transf. Distance Determ. FRET Pairs*.
67. B. C. Lin, C. P. Cheng, Z.-Q. You and C.-P. Hsu, *J. Am. Chem. Soc.*, 2005, **127**, 66–67.
68. Norman Herron and Hong Meng, in *Organic Light-Emitting Materials and Devices*, CRC Press, 2006, pp. 295–412.
69. N. K. Za'aba, M. A. M. Sarjidan, S. H. Basri and W. H. A. Majid, *J. Nanoelectron. Optoelectron.*, 2013, **8**, 437–445.
70. I. Glowacki and Z. Szamel, *J. Phys. D: Appl. Phys.*, 2010, **43**, 295101.
71. X. Jiang, R. A. Register, K. A. Killeen, M. E. Thompson, F. Pschenitzka, T. R. Hebner and J. C. Sturm, *J. Appl. Phys.*, 2002, **91**, 6717–6724.
72. S. L. Hellstrom, J. Ugolotti, G. J. P. Britovsek, T. S. Jones and A. J. P. White, *New J Chem*, 2008, **32**, 1379–1387.
73. K. Durka, S. Luliński, K. N. Jarzembska, J. Smętek, J. Serwatowski and K. Woźniak, *Acta Crystallogr. Sect. B*, 2014, **70**, 157–171.
74. Bruker AXS Inc., *APEX2*, Bruker AXS Inc., Madison, Wisconsin, USA., 2010.
75. Bruker AXS Inc., *SAINT*, Bruker–Nonius, Madison, Wisconsin, USA, 2010.
76. R. H. Blessing, *Acta Crystallogr. Sect. A*, 1995, **51**, 33–38.
77. R. H. Blessing, *J. Appl. Crystallogr.*, 1989, **22**, 396–397.
78. *CrysAlis Pro Software*, Agilent Technologies, 2010.
79. G. M. Sheldrick, *Acta Crystallogr. Sect. A*, 2008, **64**, 112–122.
80. D. Pfeifer, K. Hoffmann, A. Hoffmann, C. Monte and U. Resch-Genger, *J. Fluoresc.*, 2006, **16**, 581–587.
81. A. M. Brouwer, *Pure Appl. Chem.*, 2011, **83**, 2213–2228.
82. D.-Y. Lee, M.-H. Lee, C.-J. Lee and S.-K. Park, *Electron. Mater. Lett.*, 2013, **9**, 663–668.
83. X. Yang, D. Neher, D. Hertel and T. K. Däubler, *Adv. Mater.*, 2004, **16**, 161–166.
84. F. H. Allen and I. J. Bruno, *Acta Crystallogr. Sect. B*, 2010, **66**, 380–386.
85. M. J. Frisch, G. W. Trucks, H. B. Schlegel, G. E. Scuseria, M. A. Robb, J. R. Cheeseman, G. Scalmani, V. Barone, B. Mennucci, G. A. Petersson, H. Nakatsuji, M. Caricato, X. Li, H. P. Hratchian, A. F. Izmaylov, J. Bloino, G. Zheng, J. L. Sonnenberg, M. Hada, M. Ehara, K. Toyota, R. Fukuda, J. Hasegawa, M. Ishida, T. Nakajima, Y. Honda, O. Kitao, H. Nakai, T. Vreven, J. A. Montgomery, Jr., J. E. Peralta, F. Ogliaro, M. Bearpark, J. J. Heyd, E. Brothers, K. N. Kudin, V. N. Staroverov, T. Keith, R. Kobayashi, J. Normand, K. Raghavachari, A. Rendell, J. C. Burant, S. S. Iyengar, J. Tomasi, M. Cossi, N. Rega, J. M. Millam, M. Klene, J. E. Knox, J. B. Cross, V. Bakken, C. Adamo, J. Jaramillo, R. Gomperts, R. E. Stratmann, O. Yazyev, A. J. Austin, R. Cammi, C. Pomelli, J. W. Ochterski, R. L. Martin, K. Morokuma, V. G. Zakrzewski, G. A. Voth, P. Salvador, J. J. Dannenberg, S. Dapprich, A. D. Daniels, O. Farkas, J. B. Foresman, J. V. Ortiz, J. Cioslowski, and D. J. Fox, *Gaussian 09*, Gaussian, Inc, Wallingford CT, 2010.
86. W. Humphrey, A. Dalke and K. Schulten, *J. Mol. Graph.*, 1996, **14**, 33–38.
87. R. A. Marcus and N. Sutin, *Biochim. Biophys. Acta BBA - Rev. Bioenerg.*, 1985, **811**, 265–322.
88. P. F. Barbara, T. J. Meyer and M. A. Ratner, *J. Phys. Chem.*, 1996, **100**, 13148–13168.

Table of content:

Efficient 8-oxyquinolinato emitters based on 9,10-dihydro-9,10-diboraanthracene scaffold for applications in optoelectronic devices

Krzysztof Durka, Ireneusz Głowacki, Sergiusz Luliński, Beata Łuszczyńska, Jaromir Smętek, Paweł Szczepanik, Janusz Serwatowski, Urszula E. Wawrzyniak, Grzegorz Wesela-Bauman, Ewelina Witkowska, Gabriela Wiosna-Sałyga, Krzysztof Woźniak

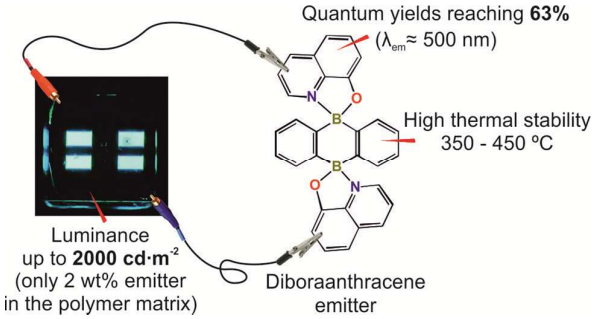

The diboraanthracene bis(oxyquinolinato) complexes exhibit green luminescence with quantum yields reaching 63%. They were employed for the construction of efficient OLEDs featuring relatively low concentration of emitter in the matrix.